Finite Volume Solution of the Two-Dimensional Euler Equations on a Regular Triangular Mesh

A. Jameson* and D. Mavriplis†
Princeton University, Princeton, New Jersey

The two-dimensional Euler equations have been solved on a triangular grid by a multigrid scheme using the finite volume approach. By careful construction of the dissipative terms, the scheme is designed to be second-order accurate in space, provided the grid is smooth, except in the vicinity of shocks, where it behaves as first-order accurate. In its present form, the accuracy and convergence rate of the triangle code are comparable to that of the quadrilateral mesh code of Jameson.

Introduction

IN the last decade, transonic flow calculations using the potential flow assumption have become fairly widespread and have proved accurate and cheap enough to be regularly used as a design tool. However, in the transonic regime the potential flow assumption is not strictly correct for it neglects the entropy and vorticity production associated with shock waves.

To describe inviscid transonic flow correctly, the Euler equations must be solved. The numerical solution of the Euler equations should provide an accurate prediction of the location and strength of a shock and the associated wave drag. Furthermore, the solution should be capable of predicting rotational flow problems such as the slip stream of a prop-fan flowing over a wing, or the flow over aircraft components in the vortex wake downstream of a wing.

Recent developments have substantially reduced the cost of Euler calculations. The finite volume formulation of Jameson et al.[1] that uses a Runge-Kutta type time-stepping scheme has proved to be robust and accurate. The rate of convergence has also been greatly enhanced by various means, including the use of a multigrid scheme.[2] It has in fact been shown in a recent paper[3] that this scheme is now sophisticated enough to be applied to complete wing/body/tail-plane/fin combinations. The next step is to apply the scheme to geometries of increased complexity, such as the addition of engine nacelle/pylon combinations to approximate the entire aircraft. The major obstacle in solving the flow problem over these increasingly complex geometries is the generation of smoothly varying meshes about the body configuration with appropriate cell distributions to calculate the flow variables over the entire body surface with sufficient accuracy. Various approaches to overcome this obstacle have been proposed, including local mesh enrichment[4] and hybrid meshes,[5] for example, a global H-mesh with imbedded O-meshes around the components of interest. Another approach is to use alternative cell geometries such as triangles or polygons. The flow solution about an entire aircraft will probably require the use of all these approaches simultaneously. This work is concerned with the use of triangular elements, which allow an added degree of flexibility in fitting complex geometries. Recently, Pelz[6] obtained the transonic potential flow solution on regular and irregular triangular grids in two dimensions, and showed how these could be applied to complex geometries not readily amenable to quadrilateral meshes.

This work represents the first demonstration of a multigrid solution scheme for the Euler equations using triangular elements. At this preliminary stage, a structured (regular) triangular grid has been used. This is seen as a necessary first step prior to solving the Euler equations on unstructured triangular meshes, which are best suited for complex geometries.

The general solution scheme is based upon that of Jameson et al.[1] and, in addition to the formulation of a multigrid scheme for a triangular grid, the efficiency of the method has been further enhanced by residual averaging and enthalpy damping.

Discretization of the Euler Equations

A regular triangular grid is constructed about an airfoil by first generating the mesh nodes for the common quadrilateral O-mesh. By shifting the appropriate nodes by half a mesh width, a mesh of symmetric triangles may be constructed by joining all of the mesh nodes with straight line segments. See Fig. 1.

The solution procedure for the Euler equations on a triangular mesh closely follows that proposed by Jameson et al.[1] for quadrilateral meshes.

The variables to be determined are the pressure, density, Cartesian velocity components, total energy, and total enthalpy, denoted by p, ρ, u, v, E, and H, respectively. Since for a perfect gas, we have the relations

$$E=\frac{p}{(\gamma-1)\rho}+\frac{1}{2}(u^2+v^2), \quad H=E+\frac{p}{\rho}$$

where γ is the ratio of specific heats, we need only solve for the four variables ρ, ρu, ρv, and ρE. These values are determined by solving the Euler equations, which in integral form read,

$$\frac{\partial}{\partial t}\int\int_{\Omega} w\,dx\,dy+\int_{\partial\Omega}(f\,dy-g\,dx)=0 \tag{1}$$

where Ω is a fixed area with boundary $\partial\Omega$, x and y the Cartesian coordinates, and

$$w=\begin{bmatrix}\rho\\ \rho u\\ \rho v\\ \rho E\end{bmatrix}, \quad f=\begin{bmatrix}\rho u\\ \rho u^2+p\\ \rho uv\\ \rho uH\end{bmatrix}, \quad g=\begin{bmatrix}\rho v\\ \rho vu\\ \rho v^2+p\\ \rho vH\end{bmatrix}$$

Received March 18, 1985; revision received Aug. 12, 1985.

*Professor, Department of Mechanical and Aerospace Engineering.
†Graduate Student, Department of Mechanical and Aerospace Engineering.

Equation (1) can be applied to each individual triangular cell. For the x momentum, for example, it yields

$$\frac{\partial}{\partial t}(S_i \rho u_i) + \sum_{k=1}^{3} (Q_k \rho u_k + \Delta y_k p_k) = 0$$

where S is the cell area, Q_k the flux velocity across side k of the cell,

$$Q_k = \Delta y_k u_k - \Delta x_k v_k$$

and Δx_k and Δy_k the increments of x and y along side k of the cell. The flow variables such as ρu_k are taken as the average of the two cell values on either side of that face. On a smooth grid, this reduces to central differencing and is second-order accurate in space. In this form, the discretization of the Euler equations leads to a system of coupled ordinary differential equations

$$\frac{\mathrm{d}}{\mathrm{d}t}(S_i w_i) + Q(w_i) = 0 \text{ for each cell } i \qquad (2)$$

where Q is the discrete approximation to the flux integral in Eq. (1).

Dissipation

As is the case with quadrilateral meshes, cell-centered Euler schemes on triangular meshes allow decoupling between the odd and even cells. In order to prevent this decoupling, extra dissipative terms are needed. Thus, Eq. (2) is replaced by

$$\frac{\partial}{\partial t}(S_i w_i) + Q(w_i) - D(w_i) = 0 \qquad (3)$$

where $D(w_i)$ must have a suitable form to damp out all undesired oscillations. In keeping with the finite volume formulation, $D(w_i)$ is constructed as a summation of fluxes across the cell faces,

$$D(w_i) = \sum_{k=1}^{3} d_{ik}$$

where d_{ik} is the flux across the face delimiting cell i and its neighbor k,

$$d_{ik} = \frac{\epsilon^{(4)}}{2}\left(\frac{S_i}{\Delta t_i} + \frac{S_k}{\Delta t_k}\right)(\nabla^2 w_i - \nabla^2 w_k)$$

The $S/\Delta t$ term is proportional to the size of the cell face ik and scales appropriately with the time derivative in Eq. (3).

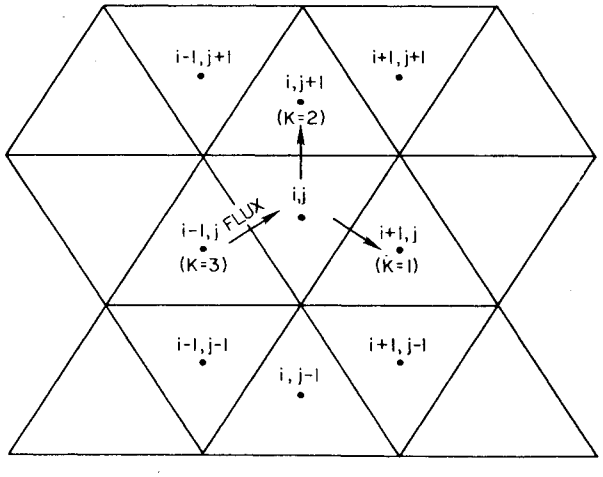

Fig. 1 Numbering scheme for a regular triangular grid.

∇^2 is the undivided four-point Laplacian operator on a two-dimensional triangular mesh,

$$\nabla^2 w_i = \sum_{k=1}^{3} w_k - 3w_i$$

and is of order $(\Delta x)^2$. Thus, the dissipative operator D is of order $(\Delta x)^3$ relative to the convective operator Q, and the accuracy of the scheme is preserved. In regions of strong pressure gradients such as near a shock wave, this dissipation is insufficient to suppress oscillations and we must add larger terms. The d_{ik} above are thus to be augmented by

$$\frac{\epsilon_{ik}^{(2)}}{2}\left(\frac{S_i}{\Delta t_i} + \frac{S_k}{\Delta t_k}\right)(w_i - w_k)$$

where $\epsilon_{ik}^{(2)}$ should be of order one near a shock and of order $(\Delta x)^2$ in regions of smooth flow where the second-order accuracy of the scheme must be preserved. One method of achieving this is to take $\epsilon_{ik}^{(2)}$ proportional to the undivided four-point Laplacian of the pressure $\nabla_{p_i}^2$. This, however, was not found to provide satisfactory behavior. If the boundary is aligned with one of the coordinate lines, pressure is exerted on it only by every second cell (see Fig. 2). Thus, we define ν_i as

$$\nu_i = \left|\frac{p_{i-2} - 2p_i + p_{i+2}}{p_{i-2} + 2p_i + p_{i+2}}\right|$$

where the subscripts j have been omitted since they are constant. In this case, $j = \text{const}$ defines the coordinate line of interest. Now μ_{ik} is defined as the maximum value of ν_i for the four cells on either side of face ik along the coordinate line $j = \text{const}$ (i.e., if face ik delimits cells i,j and $i+1,j$, μ_{ik} is the maximum of the set ν_{i-3} through ν_{i+4}). For each face ik, one of the three coordinate directions is aligned with this face and thus only two directions contain components normal to the face ik. Hence, we define

$$\epsilon_{ik}^{(2)} = k_2 \max(\mu_{ik}^{\ell}) \quad \begin{matrix} \ell = 1,2,3 \\ \text{with } \ell = k \text{ omitted} \end{matrix}$$

where μ_{ik}^{ℓ} is the μ_{ik} calculated along the coordinate line ℓ and k_2 is a constant coefficient.

In the vicinity of a shock wave, the fourth differences tend to produce overshoots; hence, they are turned off by defining

$$\epsilon_{ik}^{(4)} = \max(0, k_4 - \epsilon_{ik}^{(2)})$$

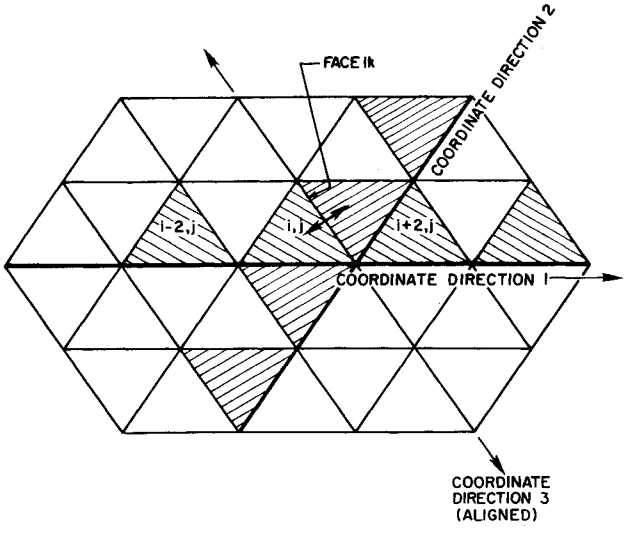

Fig. 2 Identification of the three coordinate directions for calculating the pressure switch $\epsilon_{ik}^{(2)}$.

where k_4 is a constant coefficient. The final form of the dissipative fluxes is thus,

$$d_{ik}=\frac{1}{2}\left(\frac{S_i}{\Delta t_i}+\frac{S_k}{\Delta t_k}\right)\cdot[\epsilon_{ik}^{(2)}(w_i-w_k)+\epsilon_{ik}^{(4)}(\nabla^2 w_i-\nabla^2 w_k)]$$

Time Stepping

A five-stage time-stepping scheme is used where, for economy, the dissipative operator is evaluated only in the first two stages. Since the cell volume S_i is constant, Eq. (3) may be written as

$$\frac{dw_i}{dt}+\frac{1}{S_i}[Q(w_i)-D(w_i)]=0$$

We then advance in time by the scheme

$$w^{(0)}=w^n$$

$$w^{(1)}=w^{(0)}-\alpha_1(\Delta t/S)[Q(w^{(0)})-Dw^{(0)}]$$

$$w^{(2)}=w^{(0)}-\alpha_2(\Delta t/S)[Q(w^{(1)})-D(w^{(1)})]$$

$$\vdots$$

$$w^{(5)}=w^{(0)}-\alpha_5(\Delta t/S)[Q(w^{(4)})-D(w^{(1)})]$$

$$w^{n+1}=w^{(5)}$$

where w^n and w^{n+1} are the values at the beginning and end of the nth time step. The standard values for the coefficients are

$$\alpha_1=1/4,\quad \alpha_2=1/6,\quad \alpha_3=3/8,\quad \alpha_4=1/2,\quad \alpha_5=1$$

This particular scheme is used because it is well suited to drive the multigrid algorithm. To accelerate convergence, Δt is taken as the maximum permissible local time step separately in each cell. This guarantees that disturbances will be expelled to the outer boundary in a fixed number of steps proportional to the number of cells between the inner and outer boundaries.

Boundary Conditions

The boundary conditions are those described by Jameson et al.[1] and Jameson and Baker,[3] and will be outlined only briefly here.

At the inner boundary there is no flux through the wall. However, the values of the pressure at the wall are needed to calculate the contributions $\Delta x_k\, p_k$ and $\Delta y_k\, p_k$ to the momentum equation. The wall pressure can be extrapolated from the pressure at the center of the boundary cell by use of the equations given in Ref. 1,

$$(x_X^2+y_X^2)p_Y=(x_Xx_Y+y_Xy_Y)p_X$$

$$+\rho(y_Yu-x_Yv)(vx_{XX}-uy_{XX})$$

where X and Y represent the coordinate lines aligned and normal to the boundary, and x and y are the regular Cartesian coordinates. This equation relates the normal pressure gradient at the wall due to centrifugal forces to the curvature of the boundary.

At the exterior boundary, we wish to minimize the reflection of outgoing disturbances. Consider the flow normal to this boundary. Assuming it to be locally one-dimensional, we introduce the fixed and extrapolated Riemann invariants,

$$R_\infty=q_\infty\cdot n-2c_\infty/(\gamma-1)$$

$$R_e=q_e\cdot n+2c_e/(\gamma-1)$$

corresponding to incoming and outgoing characteristics. The normal velocity and local speed of sound may thus be determined by

$$q\cdot n=\tfrac{1}{2}(R_e+R_\infty)$$

$$c=\tfrac{1}{4}(\gamma-1)(R_e-R_\infty)$$

Two other independent conditions are needed to complete the definition of the outer boundary condition. These are given by the values of tangential velocity and entropy. For an outflow boundary these are extrapolated from the interior values, whereas for an inflow boundary they are set equal to their freestream values.

Convergence Acceleration

Various devices have been employed to accelerate the convergence of the Euler equations to a steady state. One is the use of a local time step calculated from local flow properties, such that the scheme operates everywhere at its stability limit. The Euler equations themselves may also be modified for increased convergence, provided the steady-state solution is not altered. Since, in the steady state $H=H_\infty$ throughout the flowfield, it may be argued that we need not integrate the energy equation, but simply keep the enthalpy constant at its freestream value. The pressure may then be calculated from the values of density and velocity. On the other hand, we may integrate the energy equation and use the difference $H-H_\infty$ as a forcing function to accelerate convergence. Then artificial terms $\alpha\rho(H-H_\infty)$, $\alpha\rho u(H-H_\infty)$, $\alpha\rho v(H-H_\infty)$, and $\alpha\rho(H-H_\infty)$ are added to the mass, momentum, and energy equations, respectively, where α is a constant. Enthalpy damping of this type has proved effective in practice.[1]

Residual Averaging

The maximum time step that may be taken is limited by the Courant-Fredrichs-Lewy condition, which states that the domain of dependence of the discretized equations must at least contain that of the original differential equation. To ease this restriction, we may perform averaging on the residuals to increase the support of the scheme. If the residual at cell i is

$$R_i(w_i)=(1/S_i)[Q(w_i)-D(w_i)]$$

we replace it by $\overline{R_i}$,

$$\overline{R_i}=R_i+\epsilon\nabla^2 R_i$$

where ϵ is a constant and ∇^2 the four-point undivided Laplacian operator. With this procedure, it was found that the Courant number $\Delta t/\Delta x$ could be increased by about one-half, but little improvement in convergence was observed. It has been shown that on quadrilateral meshes performing the smoothing implicitly leads to infinite support and that the Courant-Fredrichs-Lewy condition no longer imposes any limit on the Courant number. Following this approach, we set

$$\overline{R_i}=R_i+\epsilon\nabla^2\overline{R_i}$$

where the barred values indicate new smoothed residuals. This may be rewritten as

$$(1+3\epsilon)\overline{R_i}-\epsilon\sum_{k=1}^{3}\overline{R_k}=R_i$$

The coefficient matrix of this system of equations contains four nonzero elements in each row and cannot be exactly inverted by an inexpensive algorithm. However, for values of ϵ in the range of interest (i.e., usually less than 1), this matrix

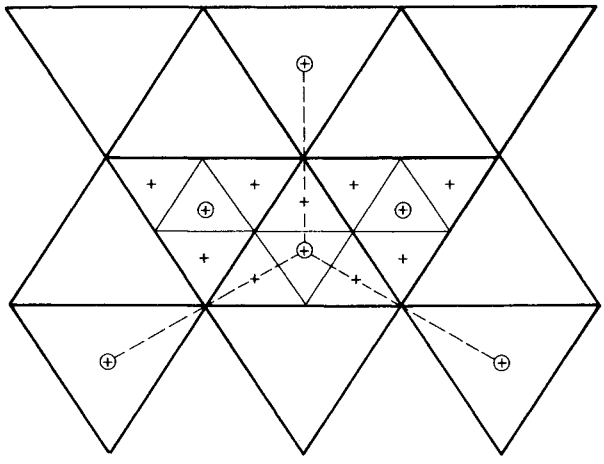

Fig. 3 Interpolation of coarse grid residuals to the fine grid.

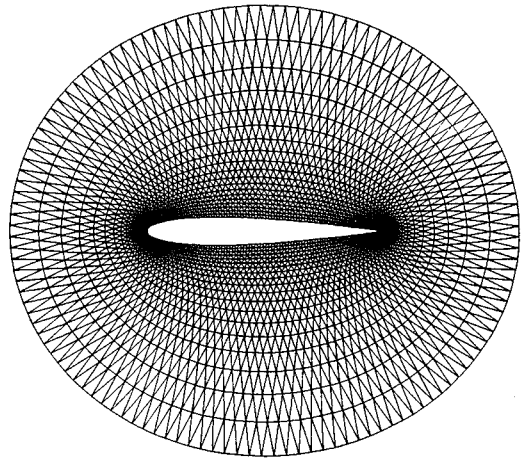

Fig. 4 128×32 regular triangular grid about a NACA 0012 airfoil.

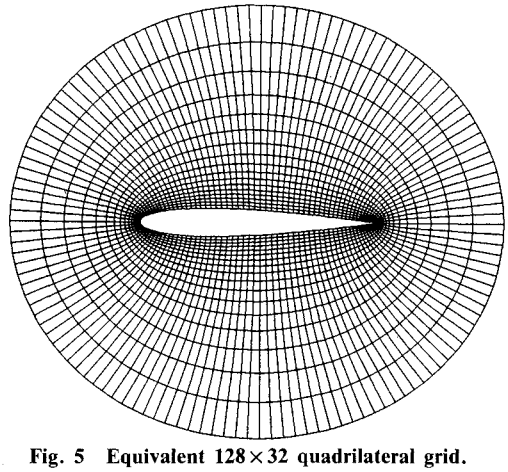

Fig. 5 Equivalent 128×32 quadrilateral grid.

is strongly diagonally dominant. Thus, an approximate solution to the R_i may be obtained by performing several Jacobi iterations on this system. In practice, ϵ is assigned the value ½ and only two iterations are required to establish the approximate values of the smoothed residuals necessary for accelerating convergence of the time-stepping scheme.

Multigrid Scheme

The idea of the multigrid scheme is to use corrections calculated on successively coarser grids to improve the solution on a fine grid. The motivation stems from the observation that the time-stepping scheme is capable of rapidly eliminating high-frequency errors, but is very slow at reducing lower-frequency or global errors. Since the highest-frequency errors which are visible to a particular grid are of the order of one mesh width, time stepping on progressively coarser grids will have the effect of rapidly eliminating a distinct bandwidth of errors on each grid.

The five-stage scheme is used to drive the multigrid algorithm because it has excellent high-frequency damping properties. For a regular triangular mesh, coarser grids may be constructed by doubling the mesh width and assembling groups of four small triangles to form one large triangular cell (Fig. 3). The flow variables are transferred to the coarser grid by the rule

$$w_{2h}^{(0)} = \Sigma (S_h w_h)/S_{2h}$$

where the subscripts denote the mesh spacing. S is the cell area and the sum is over the four triangles composing each cell on the coarse grid. This rule conserves mass, momentum, and energy. We may similarly sum the fine grid residuals to obtain

$$R_{2h}^{(0)} = \Sigma R_h (w_h)$$

Our objective is to find a correction δw such that

$$\Sigma R_h (w + \delta w) = 0$$

Remembering that the residual is a nonlinear function of w, we approximate this as

$$R_{2h}(w_{2h} + \delta w) - R_{2h}(w_{2h}) + R_{2h}^{(0)} = 0 \qquad (4)$$

where $(\partial R_{2h}^{(0)}/\partial w)\delta w$ has been replaced by the corresponding difference on the coarse grid. Since the left-hand side of Eq. (4) is the quantity we wish to minimize, we advance in time on the coarse grid as follows

$$w_{2h}^{(q+1)} = w_{2h}^{(0)} - \alpha_q \Delta t [R_{2h}(w_{2h}^{(q)}) - R_{2h}(w_{2h}^{(0)}) + R_{2h}^{(0)}]$$

for the qth stage of the time-stepping scheme. Thus, time stepping on the coarse grid proceeds as on the fine grid, except for the addition of the forcing function

$$R_{2h}^{(0)} - R_{2h}(w_{2h}^{(0)})$$

This may be repeated on successively coarser grids. On returning from the coarse to the fine grid, it is found that each fine grid cell center lies on a straight line that joins two coarse grid cell centers; the corrections are, therefore, linearly interpolated between the two coarse grid cell centers. This is illustrated in Fig. 3.

An effective multigrid strategy is to calculate one time step on each grid when passing to coarser grids and simply to interpolate the flow variables without time stepping when returning to finer grids.

In practice, computations begin by imposing a uniform flowfield over the entire grid. At time $t=0$, the airfoil is impulsively introduced by suddenly requiring that the boundary condition at its surface be satisfied. The Euler equations are then integrated in time until a steady state is reached. Convergence can thus be monitored by the average size of the residuals in the flowfield. At each stage in a single time step, the convective operator Q is recalculated and the dissipative operator D is either recalculated or taken as that of the previous stage. The resulting residuals are then smoothed and the flow variables are updated by the time-stepping scheme. After all stages of the time step are completed, the flow variables are modified by introducing the enthalpy damping terms.

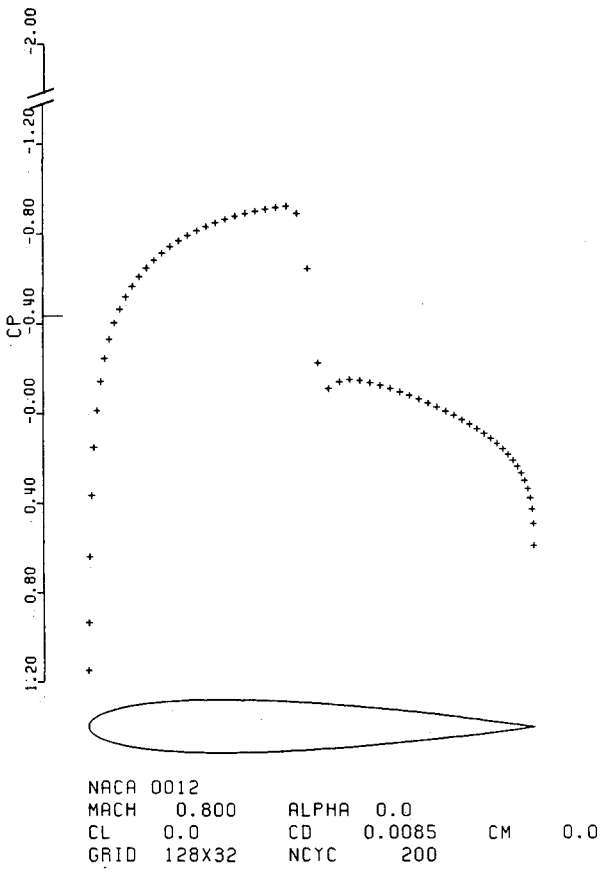

Fig. 6 Calculated pressure distribution using triangle code.

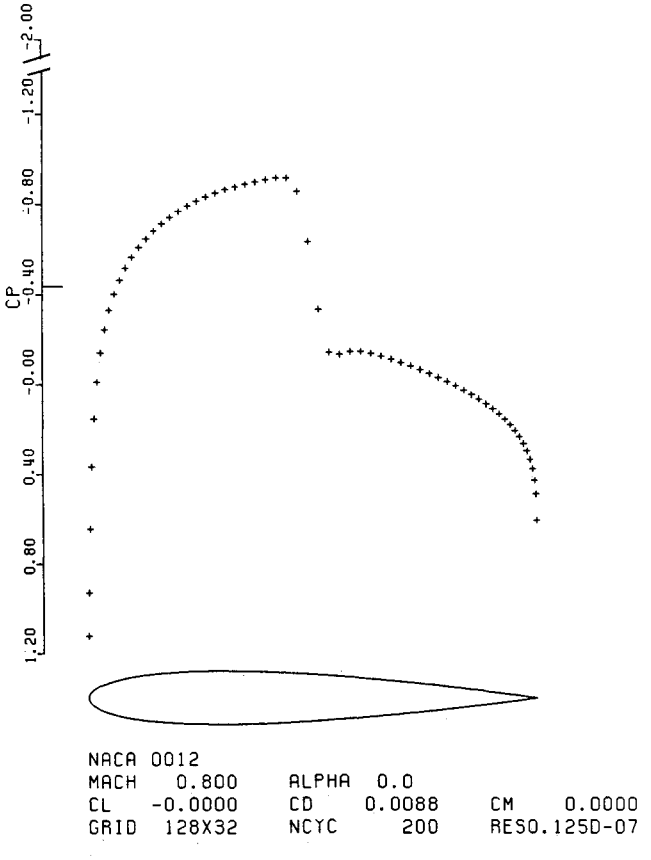

Fig. 7 Calculated pressure distribution using FL052.

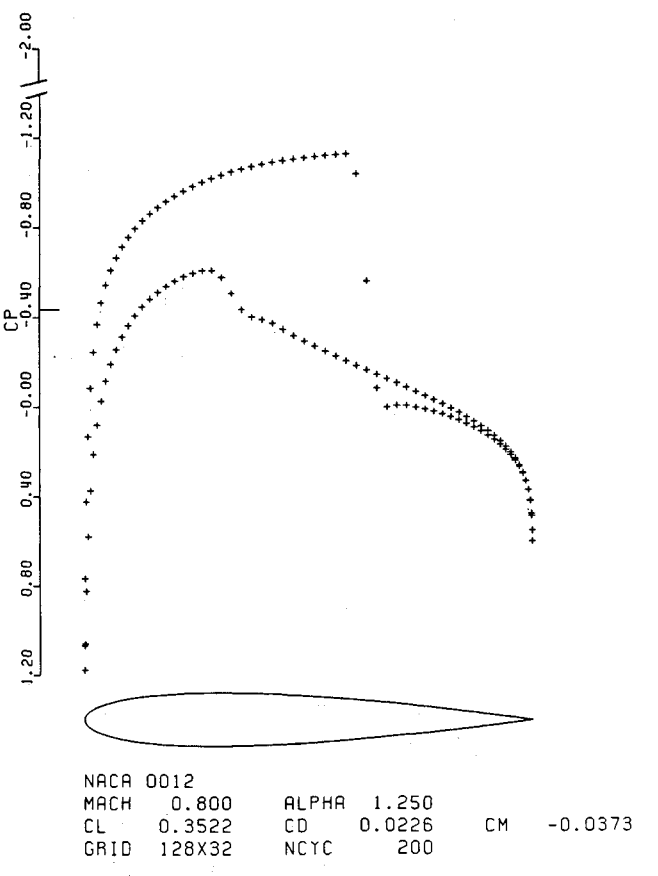

Fig. 8 Supercritical lifting case.

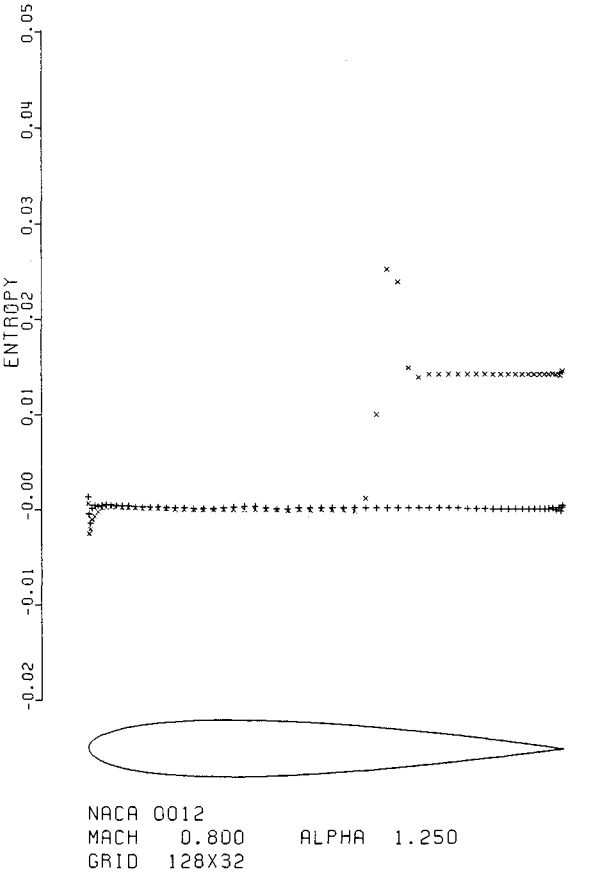

Fig. 9 Surface entropy plot for the supercritical lifting case.

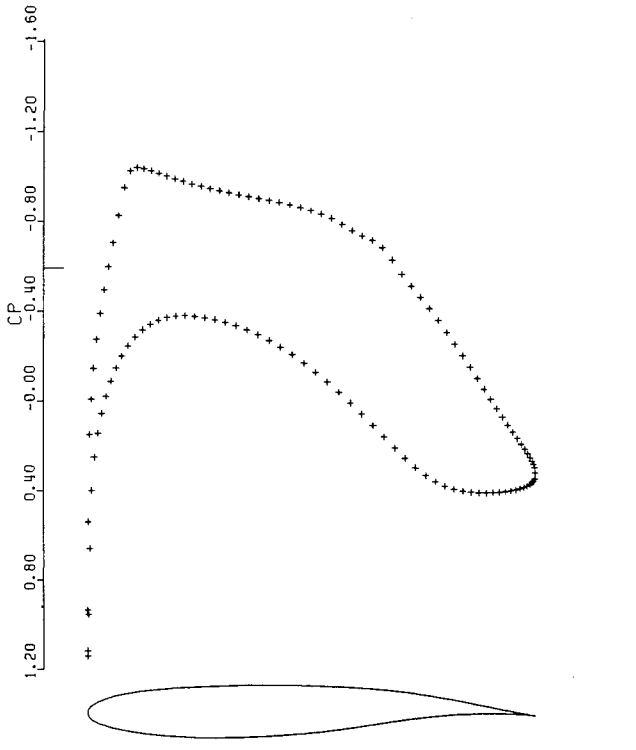

Fig. 10 KORN airfoil.

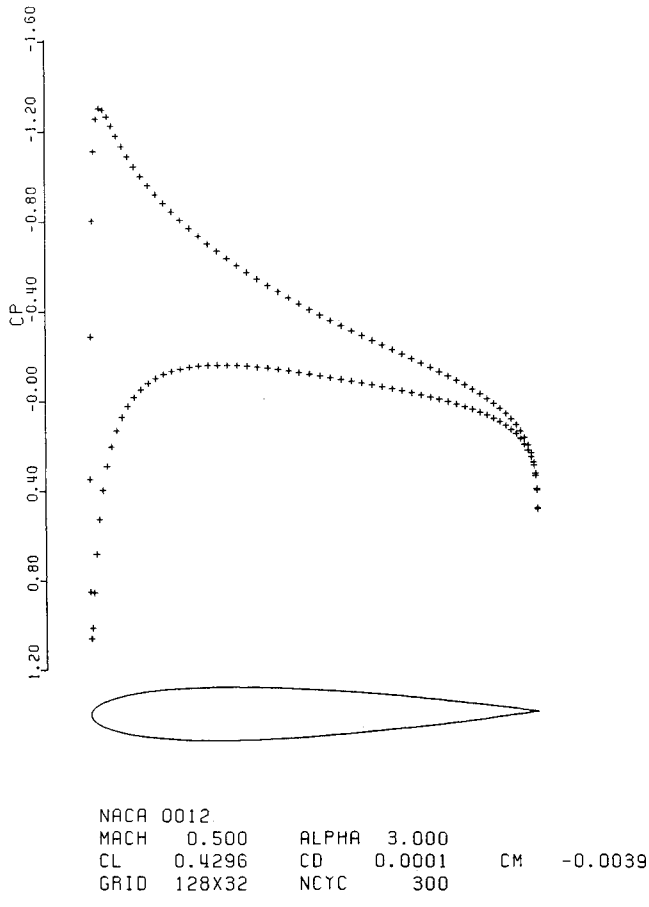

Fig. 11 Subcritical lifting case.

Time stepping on all grids uses the same Courant number along with a variable time step and identical residual averaging. Enthalpy damping is confined to the finest grid, while the dissipative operator D is modified for economy on the coarse grids to a first order accurate form, which simply uses second differences with a fixed coefficient.

Results

A typical triangular-element O-mesh about an airfoil is shown in Fig. 4. The grid contains 128 nodes around the airfoil and 32 in the radial direction. We refer to it as a 128×32 grid, although there are actually 256×32 triangular elements. The equivalent quadrilateral O-mesh with the same number of mesh nodes is depicted in Fig. 5. Figure 6 shows the calculated pressure distribution about a NACA 0012 airfoil at 0 deg angle of attack and Mach number 0.8. The artificial dissipation is successful in eliminating any preshock oscillations and the calculated value of the drag coefficient of 0.0085 agrees almost exactly with that obtained from a calculation of using FL052, an Euler solver on an equivalent quadrilateral mesh (see Fig. 7). Note that this value also agrees closely with the experimentally observed increase in drag (i.e., net wave drag) at this Mach number over the subcritical value for C_D (mainly viscous drag).

A supercritical lifting case is shown in Fig. 8 where the NACA 0012 airfoil has been given an angle of attack of 1.25 deg at the same Mach number. A plot of the surface entropy for this case is given in Fig. 9, where the entropy jump across the strong upper surface shock is clearly visible and the small lower surface shock is seen to be essentially isentropic. Figure 10 shows the calculated pressure distribution about a KORN airfoil at 0 deg angle of attack and Mach number of 0.75. Morawetz' theorem[7] guarantees that any shock-free solution in transonic flow is an isolated point. The KORN airfoil is designed by the hodograph method to attain such a shock-free

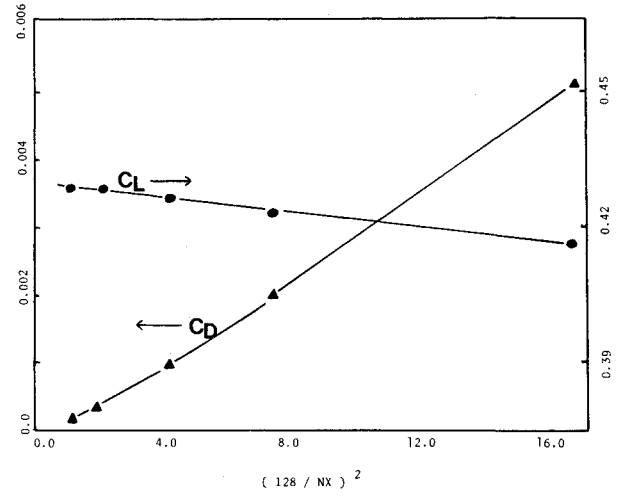

Fig. 12 Calculated force coefficients as a function of mesh width for the subcritical lifting case.

solution at the above conditions. Thus, the shock-free solution obtained numerically and shown in Fig. 10 is a strong indication of the accuracy of the scheme. Finally, a subcritical lifting case is shown in Fig. 11 where the drag is seen to be virtually zero, as expected. The lift and drag coefficients for all these cases agree to within three decimal places with those calculated using FL052.

For subcritical cases, where no shock waves are present, the scheme should be second-order accurate provided that the grid is smooth enough. Furthermore, since the flow will be irrotational, the drag should be zero, and the calculated

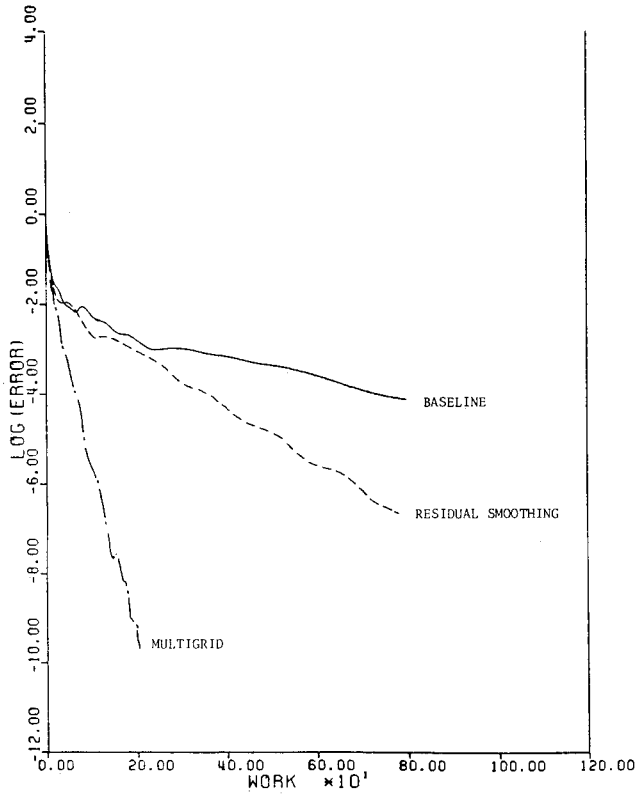

Fig. 13 Convergence acceleration as measured by the rms value of $(\partial\rho/\partial t)$ (density residual).

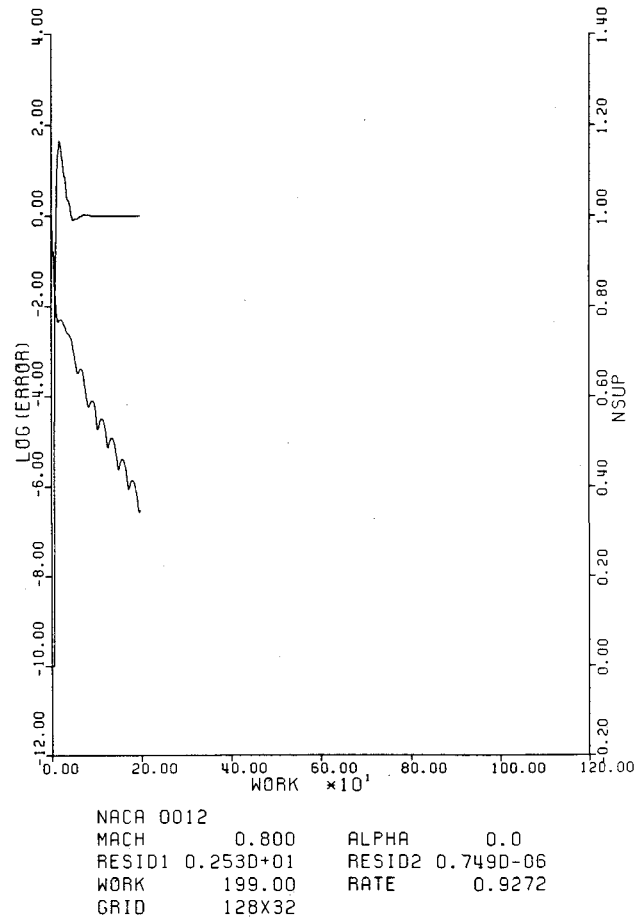

Fig. 14 Convergence rate of multigrid triangle code as measured by the rms value of $(\partial\rho/\partial t)$ (density residual) and buildup of supersonic points.

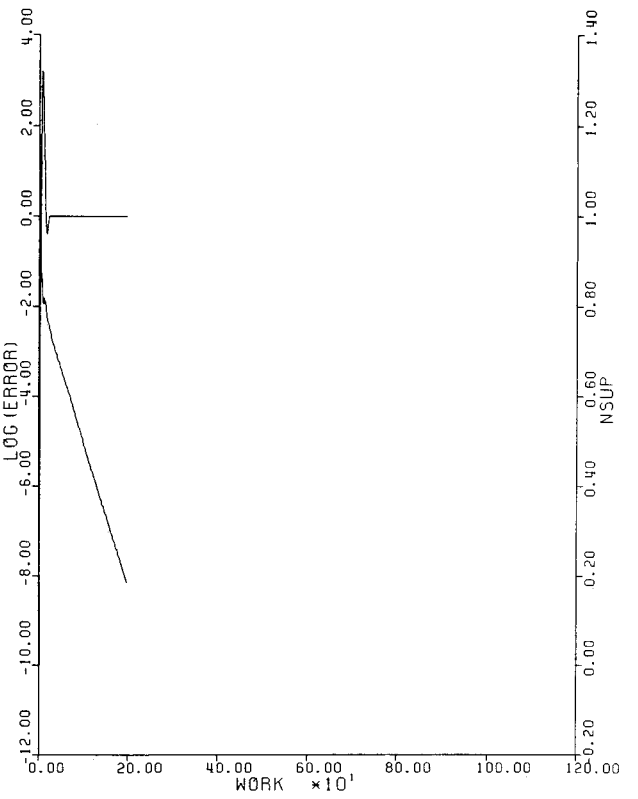

Fig. 15 Convergence rate of FL052.

value of C_D may provide an estimate of the discretization error. The subcritical lifting case of a NACA 0012 airfoil at Mach number 0.5 and 3 deg angle of attack has been run for various grid sizes and the values of C_L and C_D are plotted in Fig. 12 as a function of the square of the mesh width. These results plot as straight lines and thus verify the second-order accuracy of the scheme.

The convergence rate of the triangle code for a supercritical case on a coarser 64×16 mesh is depicted in Fig. 13 where the improvements due to residual averaging and the multigrid scheme are shown. Figures 14 and 15 provide a comparison of overall convergence rates of the triangle code and FL052 on 128×32 meshes. The average residual reduction per multigrid cycle of 0.9272 for the triangle code is somewhat slower than that achieved on quadrilaterals. However, it must be recalled that the triangular element mesh has twice as many cells as the quadrilateral mesh.

Thus, the calculations verify that on equivalent meshes solutions can be achieved with similar accuracy and convergence rates using either triangular or quadrilateral elements. On a triangular mesh, discretization errors that depend on the distance between cell centers arise when flow variables between two centers are taken as the average of the two values at these centers. However, discretization errors that depend on the size of the cell face also arise due to approximations when integrating around the boundary of the cell. If a given area is covered by N quadrilaterals with cell spacing h, then $4/3\sqrt{3}\ N$ equilateral triangles are required to cover the same area, if an equal spacing h is maintained between the cell centers. On the other hand, if we retain the same side length h, then $4/\sqrt{3}\ N$ equilateral triangles are required. Thus, we cannot precisely characterize a triangular mesh of equivalent accuracy to a given quadrilateral mesh. The numerical calculations used twice as many elements in

the triangular mesh. In subcritical cases, the triangle scheme also realized greater accuracy, as measured by the drag coefficient, suggesting that the size of the triangles could have been increased for equivalent accuracy. Also, the amount of computation is reduced by the need to calculate fluxes on three rather than four sides per cell.

Conclusions and Further Work

Comparable convergence rates have been demonstrated for the triangular and rectangular grids and we conclude that for a given desired accuracy as measured by the calculated force coefficients, Euler solutions can be obtained on either type of grid with roughly the same amount of computing effort.

The existing code is presently being rewritten in a more general form, using an indirect addressing system to locate cell centers and their corresponding mesh nodes, in order to allow the use of completely irregular meshes. Another version in which the flow variables are stored at the cell corners is also under development. Planned extensions of this work include patching of triangular grids with quadrilateral grids and extension to three-dimensional grids with triangular prisms or tetrahedra.

References

[1]Jameson, A., Schmidt, W., and Turkel, E., "Numerical Solution of the Euler Equations by Finite Volume Methods Using Runge-Kutta Time Stepping Schemes," AIAA Paper 81-1259, 1981.

[2]Jameson, A., "Solution of the Euler Equations by a Multigrid Method," *Applied Mathematics and Computation*, Vol. 13, 1983, pp. 327-356.

[3]Jameson, A. and Baker, T. J., "Solution of the Euler Equations for Complex Configurations," *Proceedings of AIAA 6th Computational Fluid Dynamics Conference*, AIAA, New York, 1983, pp. 293-302.

[4]Berger, M. J. and Jameson, A., "Automatic Adaptive Grid Refinement for the Euler Equations," Princeton University, Princeton, NJ, MAE Rept. 1633, Oct. 1983.

[5]Vermeland, R. E., "Solution of the Two-Dimensional Euler Equations on a Hybrid Mesh," Princeton University, Princeton, NJ, MAE Rept. 1679, Aug. 1984.

[6]Pelz, R. B., "Transonic Flow Calculations Using Finite Elements," Ph.D. Thesis, Princeton University, Princeton, NJ, 1983.

[7]Morawetz, C. S., "On the Non-Existence of Continuous Transonic Flows Past Profiles," *Communications on Pure and Applied Mathematics*, Vol. 9, 1956, pp. 45-48.